Paleoceanography and Paleoclimatology

RESEARCH ARTICLE
10.1029/2020PA004184

Key Points:

- Centennial-scale hydroclimate variability in the Northern Bahamas is anti-phased with mid-late Holocene hydroclimate over Grenada and Barbados
- Evidence is presented for a Caribbean hydroclimate dipole caused by meridional displacements of the North Atlantic Subtropical High
- Calcite raft sedimentation in sinkholes and caves on carbonate landscapes offers new opportunities to investigate rainfall variability

Supporting Information:

Supporting Information may be found in the online version of this article.

Correspondence to:

R. M. Sullivan,
richardmsullivan@tamu.edu

Citation:

Sullivan, R. M., van Hengstum, P. J., Coats, S. J., Donnelly, J. P., Tamalavage, A. E., Winkler, T. S., & Albury, N. A. (2021). Hydroclimate dipole drives multi-centennial variability in the western tropical North Atlantic margin during the middle and late Holocene. *Paleoceanography and Paleoclimatology*, *36*, e2020PA004184. https://doi.org/10.1029/2020PA004184

Received 7 DEC 2020
Accepted 30 JUN 2021

Hydroclimate Dipole Drives Multi-Centennial Variability in the Western Tropical North Atlantic Margin During the Middle and Late Holocene

Richard M. Sullivan[1], Peter J. van Hengstum[1,2], Sloan J. Coats[3], Jeffrey P. Donnelly[4], Anne E. Tamalavage[1], Tyler S. Winkler[1], and Nancy A. Albury[5]

[1]Department of Oceanography, Texas A&M University, College Station, TX, USA, [2]Department of Marine and Coastal Environmental Science, Texas A&M University at Galveston, Galveston, TX, USA, [3]Department of Earth Sciences, University of Hawaii, Honolulu, HI, USA, [4]Coastal Systems Group, Woods Hole Oceanographic Institution, Woods Hole, MA, USA, [5]National Museum of The Bahamas, Nassau, Bahamas

Abstract Meridional shifts of the North Atlantic Subtropical High (NASH) western edge create a dipole that drives hydroclimate variability in the southeastern United States and Caribbean region. Southwest displacements suppress rainfall in the southern Caribbean. Northwest displacements drive southeast United States and northern Caribbean drying. Projections for the 21st century suggest a more meridionally displaced NASH, which jeopardizes Caribbean island communities dependent on rain-fed aquifers. While recent work indicates that Atlantic and Pacific Ocean-atmosphere variability influenced the NASH during the instrumental period, little is known about NASH behavior and subsequent hydroclimate responses over longer timescales. To address this limitation, we developed a ~6000-years long rainfall record through the analysis of calcite raft deposits archived within sediments from a coastal sinkhole in the northeast Bahamas (Abaco Island). Increased (decreased) calcite raft deposition provides evidence for increased (decreased) rainfall driven by NASH variability. We use simulations from the Community Earth System Model to support this interpretation. These simulations improve our understanding of NASH behavior on timescales congruous with the reconstruction and suggest an important role for the state of the Pacific Ocean. Furthermore, model simulations and a compilation of regional hydroclimate reconstructions reveal that the NASH-driven dipole dominates northern and southern Caribbean rainfall on centennial timescales. These results bring Holocene Caribbean hydroclimate variability into sharper focus while providing important context for present and future changes to regional climate. Additionally, this study highlights the need for improved future predictions of the state of the Pacific Ocean to best inform water scarcity mitigation strategies for at-risk Caribbean communities.

1. Introduction

Multiple factors regulate rainfall and evapotranspiration in the Intra-American Seas (IAS, the region including the tropical and subtropical Northwest Atlantic, Caribbean, and the Gulf of Mexico); such as the Intertropical Convergence Zone (ITCZ), Caribbean Low-Level Jet (CLLJ), Pacific and Atlantic sea surface temperature (SST) teleconnections, and the North Atlantic Subtropical High (NASH; Gamble et al., 2008; L. Li et al., 2012; Martin & Schumacher, 2011; Martinez et al., 2019). The interacting pathways by which these factors influence hydroclimate throughout the IAS may manifest regionally as intervals of prolonged rainfall or persistent drought. Drought poses a significant risk to developing countries and small island nations (Karnauskas et al., 2016), which are often dependent on rain-fed carbonate aquifers for potable water (Hay et al., 2013; Kelman & West, 2009; Pelling & Uitto, 2001). The United Nations Economic Commission reports nearly $100B USD in climate-related losses between 2000 and 2018 for Caribbean small island developing states (retrieved from, https://estadisticas.cepal.org/cepalstat/portada.html). Drought frequency and duration are expected to increase throughout the region over the 21st century (Easterling et al., 2017; Naumann et al., 2018; Prudhomme et al., 2014), further depleting rainfed groundwater resources and enhancing current water stresses. Furthermore, projections for the southeastern United States and Caribbean indicate an increase in extreme precipitation events despite an overall decrease in annual precipitation amounts (Ashfaq et al., 2016; McLean et al., 2015).

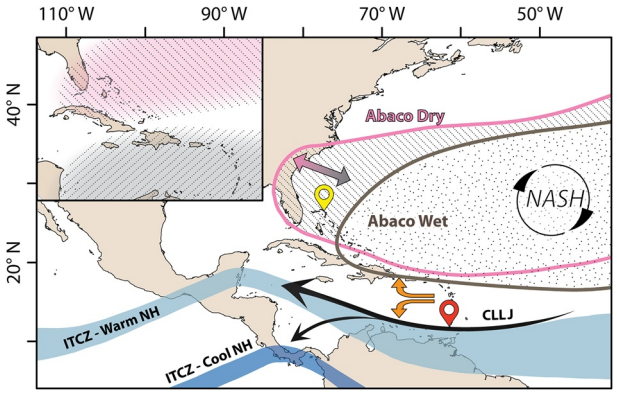

Figure 1. Conceptual Model showing the relevant hydroclimate controls in the Caribbean. Main Panel: A southerly shifted North Atlantic Subtropical High (NASH) western edge (in gray) amplifies the flow of the Caribbean Low-Level Jet, which increases divergence (orange arrows) over the Lesser Antilles and Southern Caribbean. A northern displacement of the NASH western edge (pink) suppresses rainfall in Abaco (in yellow) and decreases divergence over Barbados and Grenada (red). A more northerly position (or extent) of the Intertropical Convergence Zone (light blue) increases moisture delivery to the southern Caribbean, while a southern extent minimizes moisture delivery (dark blue). NASH positions adapted from modern observations. Inset panel: Shaded hatched areas highlight Intra-American Seas regions impacted by the hydroclimate dipole as discussed in this study.

1.1. Controls on Modern IAS Climate

In general, rising humid air in the ITCZ drives tropical rainfall while subsequent poleward advection causes cool dry air to descend at the subtropical extent of the North Atlantic Hadley cell. The NASH, which is a high-pressure anti-cyclone associated with Coriolis forcing on the Hadley cell's descending branch, drives midlatitude aridity in the North Atlantic (Lu et al., 2007; Scheff & Frierson, 2012) by increasing divergence, inhibiting convection, and deflecting precipitable moisture (Gamble et al., 2008; Hastenrath, 1976, 1984; Martinez et al., 2019). The CLLJ transports humid air associated with the ITCZ from lower latitudes throughout the Caribbean and into Central America (Martin & Schumacher, 2011). Intensification of the CLLJ can suppress convection in the southern Caribbean by stabilizing the atmospheric boundary layer and increasing local moisture divergence (Figure 1). The strength of the CLLJ is closely linked to the expansion and contraction, as well as locational shifts, of the NASH. Additionally, the Atlantic Meridional Overturning Circulation (AMOC) modulates Atlantic ITCZ behavior and the phase of the Atlantic Multi-decadal Oscillation (AMO) through cross-equatorial ocean heat transport (Moreno-Chamarro et al., 2020), but AMOC-induced changes to hydroclimate may exhibit multi-annual or decadal time lags (Moreno-Chamarro et al., 2020).

Of particular interest to IAS hydroclimate is a meridional hydroclimate dipole between ~10° and ~30°N driven by geographic displacements of the NASH western edge and primarily expressed in the boreal summer. Defining the western edge of the NASH as the 1,560 gpm isoline of the 850 hPa geopotential height, L. Li et al. (2012) documented how the dipole impacted regional rainfall between 1948 and 2007: (a) northwest displacement of the NASH western edge generally decreased precipitation in the southeastern United States and northern Caribbean while precipitation increased in the southern Caribbean, (b) southwest displacement suppressed rainfall in the southern Caribbean while increasing rainfall in the southeastern United States and northern Caribbean (Figure 1). In this configuration, a southwesterly displaced NASH inhibits convection and increases moisture divergence in the southern Caribbean via an associated strengthening of the CLLJ (Cook & Vizy, 2010). Additionally, a southwest displaced NASH increases moisture advection along its western edge from the eastern equatorial Pacific region/southwest IAS to the northeast IAS (Martinez et al., 2019).

Displacements of the NASH western edge are closely related to spatial variability in the NASH itself. Contemporary observations reveal that northern hemispheric warming encourages NASH expansion through increased land/sea thermal gradients (W. Li et al., 2012), while in contrast, positive phases of the AMO lead to NASH contraction and general northward displacement (Hu et al., 2011) by reducing these land/sea gradients. Negative phases of the AMO encourage both a westward shift and NASH intensification (i.e., strengthening and expansion). Notwithstanding changes in the position of the NASH, NASH intensification also encourages a southwestward displacement of the western edge (W. Li et al., 2012). Teleconnections related to the positive phase of the Pacific Decadal Oscillation (PDO) are thought to encourage northwest shifts in the location of the NASH western edge (L. Li et al., 2012). Coupled Model Intercomparison Project Phase 3 (CMIP3) experiments forecast that NASH intensification and southwest displacements will become more frequent in the coming century from increased land-ocean thermal contrasts (Kelly et al., 2018; L. Li et al., 2012; W. Li et al., 2012). Despite the breadth of work done to understand contemporary NASH dynamics, little is known about how the NASH and the associated IAS hydroclimate dipole varies on longer timescales.

1.2. Holocene Paleoclimate Records From the Northern IAS

Centennial-to-millennial scale patterns in NASH behavior can be assessed using suitable paleoclimate proxy archives sensitive to regional hydroclimate change. Located in the northeast IAS and proximal to the

southeast United States. The Bahamas is a key locality to evaluate NASH behavior because the archipelago is vulnerable to hydroclimate impacts from meridional displacements of the NASH western edge. Problematically, available paleoclimate studies for the northeast IAS are often insufficient for the characterization of long-term climatological variability. They may lack sufficient temporal resolution (van Hengstum et al., 2018), record only pre-Holocene conditions (Arienzo et al., 2015), or are biased by late-Holocene anthropogenic land-use modifications and thus not faithful archives of natural landscape-climate interactions (Fall et al., 2021; Kjellmark, 1996; Slayton, 2010). $\delta^{18}O$ records from Dos Anos cave in western Cuba (Fensterer et al., 2013) and δD from plant waxes on Abaco (Tamalavage et al., 2020) are likely responsive to the synoptic-scale variations in moisture source that subtend local rainfall, and thus these records may not exclusively reflect local precipitation patterns over the Bahamas. While there are hydroclimate reconstructions further south in the IAS that may avoid these caveats (Fritz et al., 2011; Haug et al., 2001; Hodell et al., 1991; Mangini et al., 2007), long-term hydroclimate records sensitive to local rainfall variability are scant for the northern IAS region proximal to the western boundary of the NASH.

Previous studies, including both numerical modeling (Bartlein et al., 1998; Kelly et al., 2018) and multi paleo-proxy analysis (Mayewski et al., 2004; Routson et al., 2019), have disagreed over the prevalent hydroclimate conditions in the wider IAS basin during the mid-Holocene (~6,000–5,000 yBP). Through a multi-proxy synthesis, Mayewski et al. (2004) identified a regional pattern of increasing or elevated precipitation. Others have suggested that during the mid-Holocene, the tropical Northwest Atlantic should have been drier than present (Kelly et al., 2018) or highly variable (Routson et al., 2019). These discrepancies may result from the focus on solar forcing of North Atlantic rainfall independent of other mechanisms (Kelly et al., 2018) or the limited number of paleo records available for the tropical North Atlantic (Routson et al., 2019). While these lower spatial and temporal resolution paleo-proxy syntheses remain relevant, they can average out regionally specific variability, as evidenced over the instrumental period (Jury et al., 2007). Such regional nuance is best captured in locally derived hydroclimate records.

To address these deficiencies, we developed a sediment-based hydroclimate reconstruction from a sinkhole lake on Abaco Island (26°N, 77°W). Abaco is the easternmost island on Little Bahama Bank, which is the northernmost carbonate platform along the western tropical North Atlantic margin (Figure 2). Rainfall in the northern Bahamas is highly sensitive to NASH behavior during the summer wet season (MJJASO). A precipitation record spanning 1855 to 2017 CE from nearby New Providence Island, which is in the same hydroclimate zone as Abaco Island (Jury et al., 2007), shows that ~75% of the mean annual rainfall occurs during the summer wet season (Figure 2e). This suggests that lower-resolution paleoclimate records sensitive to rainfall amount but unable to distinguish seasonal cycles are most likely indicative of summertime rainfall variability, and by proxy, long-term NASH behavior. The reconstruction spans ~7,300–1,800 yBP and captures prominent arid and pluvial intervals in the region. These intervals are anti-phased from hydroclimate changes in the southern Caribbean and suggest that a regional hydroclimate dipole operates on at least multidecadal timescales. This new record is compared with simulations from the Community Earth System Model (CESM) to better understand NASH behavior at these timescales. Specifically, the CESM allows us to quantify the influence of large-to-regional scale climate variability on NASH western edge position, the NASH as a whole, and regional rainfall. These analyses reveal the dominant factors driving variability in the NASH western edge, and thus, the hydroclimate dipole.

2. Study Site and Methods

2.1. Great Cistern Sinkhole and Sediment Cores

Great Cistern is a groundwater-fed, ~15 m diameter sinkhole lake located 35 m inland from the eastern Abaco shoreline, and is ~1.5 m above sea level (Figure 2). The sinkhole has an average water depth of 9 m, though the depth does increase gradually from the northeast to the southwest, where a maximum of 11 m was recorded. A pycnocline at 8 m divides an upper brackish and oxygenated water mass (surface dissolved oxygen: 6 mg l^{-1}, salinity: 10 psu), from a lower dysoxic water mass (benthos dissolved oxygen: 0.1 mg l^{-1}, salinity: 20 psu, as measured with a YSI EXO1 water quality sonde, Figure S1). Sediment cores were collected from Great Cistern using push coring (C2) and a submersible Rossfelder P3 vibracore (C7 and C8) (Figure 3; Sullivan et al., 2020). It is likely that the entire unlithified sedimentary infill was

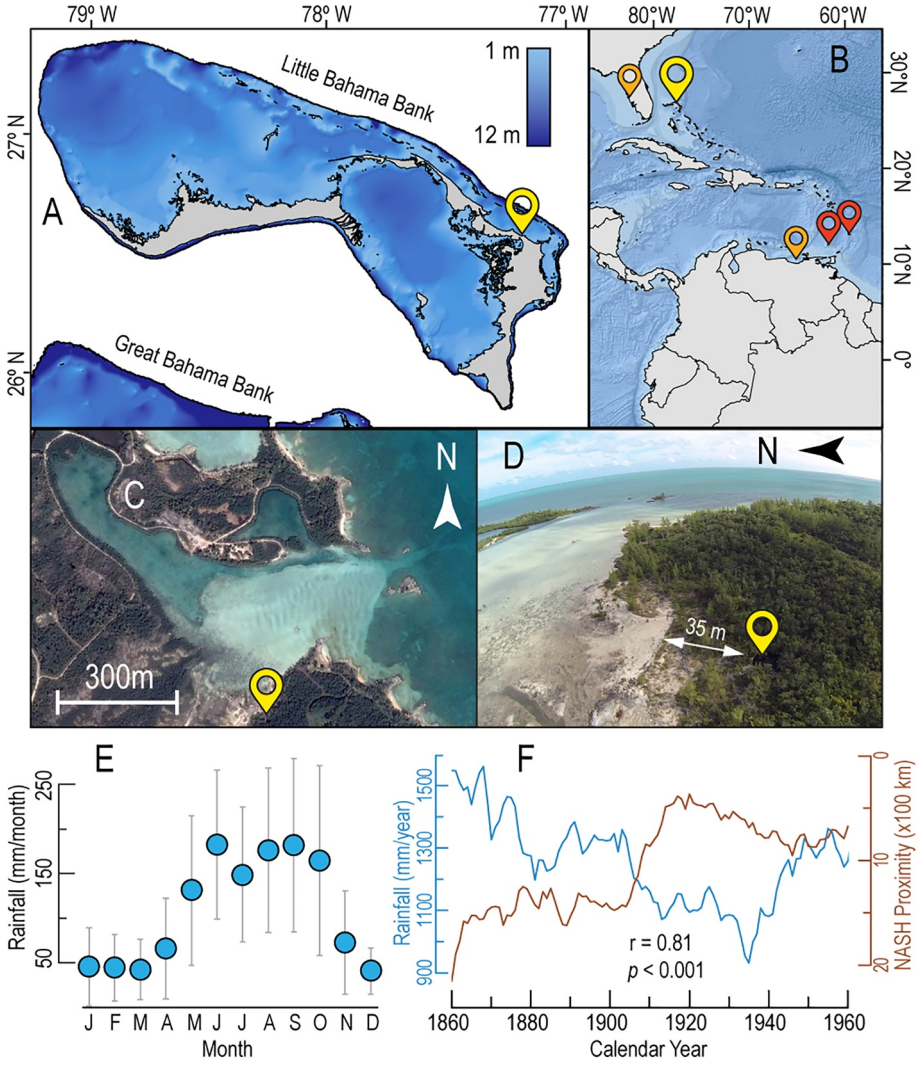

Figure 2. (a) Little Bahama Bank. Great Cistern sinkhole is shown in yellow. (b) Tropical Northwest Atlantic and Caribbean basin. Referenced paleo records marked in red (Grenada and Barbados) and orange (Cariaco Basin, Venezuela, and Brown's Cave FL). (c, d) Great Cistern sinkhole is located ~35 m from the current shoreline on eastern Abaco Island. (e) Average monthly rainfall from the Nassau rain gauge (1855–2017). Bars denote 1σ interval. Suppressed July rainfall indicates the recurrent mid-summer drought. (f) Annual rainfall totals from the Nassau rain gauge (blue) and NASH proximity (brown) smoothed by a 4-year running mean from 1860 to 1960. Note that the increases in precipitation in 1927–1929 despite a proximal NASH were the result of tropical cyclones impacting Nassau in September and October of those years. The rainfall delivered by these storms offset the annual totals for what were otherwise anomalously dry years.

sampled because vibracoring beyond a depth of 485 cm was prevented by an impenetrable substrate. C7 (435 cm) captured the near-complete Holocene sequence, though the upper 50 cm were not recovered. C8 recovered the stratigraphy from the sediment-water interface to a depth of 352 cm. C2 (236 cm) sampled to a depth of 250 cm below the sediment-water interface, though the upper 14 cm were lost due to over-penetration. After transport back to the laboratory, the cores were sectioned lengthwise, described, photographed, and X-radiographed. In addition, C2 was scanned using an ITRAX x-ray fluorescence (XRF) core scanner at 1 mm intervals. The X-radiographs document excellently preserved horizontal bedding throughout all cores (Figure 3), which indicates negligible vertical sediment mixing from biological or physical action.

The Sieve-First Loss-on-Ignition (LOI) procedure was used to quantify coarse-grained particle deposition downcore, which is a modification to the classic LOI procedure. Sieve-First LOI is well-suited for quantifying

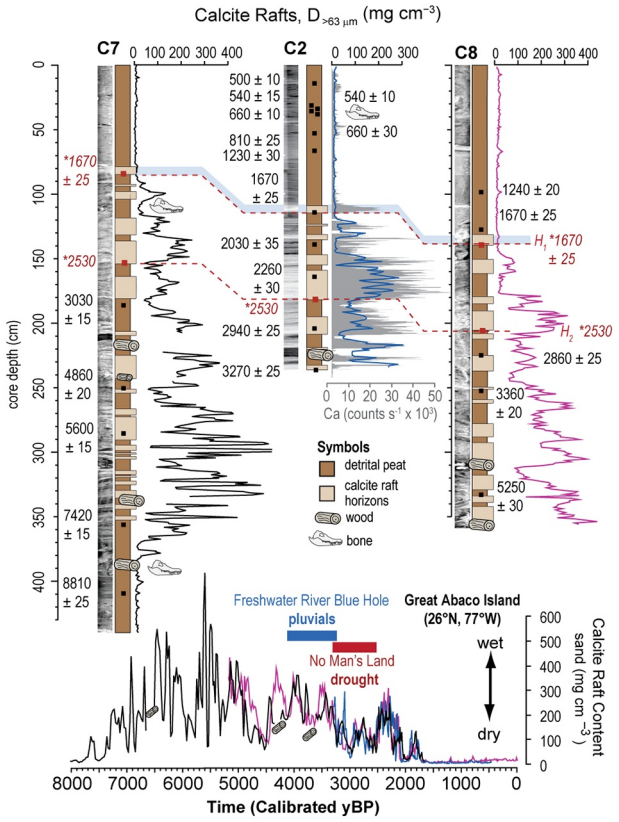

Figure 3. (Top) Downcore stratigraphic variability, including lithologic changes, and coarse-grained particle content. For the radiocarbon dates, only the highest probability 1σ calibration result is depicted. Red dates indicate stratigraphic tie points (H1 and H2) used to correlate coarse beds represented in all three cores (see supporting information). (bottom) Coarse data for all three cores plotted against the Bayesian age/depth results. For discussion of faunal remains, see Sullivan et al. (2020).

coarse grain deposition in carbonate lakes on limestone landscapes (van Hengstum et al., 2016, 2018). Sediment sub-samples (2.5 cm^{-3}) were obtained at contiguous 1 cm intervals for all three cores. Samples were first wet sieved over a 63 μm mesh, desiccated at 80°C for 24 h, weighed post-desiccation, and then combusted at 550°C for 4.5 h to remove organic matter and concentrate any remaining sand-sized mineral particles. Post-combustion weights are used to quantify the variability in coarse-grained particle deposition downcore expressed in mass per unit of volume ($D > 63$ μm mg cm^{-3}). Coarse-grained particles were identified as a form of calcite morphology known as "calcite rafts" (see Section 3.2). Scanning electron microscopic (SEM) images of representative calcite raft fragments (Figure 4) were collected with a Hitachi TM3000 tabletop scanning electron microscope. Sediment age control was established by radiocarbon dating terrestrial plant macrofossils (e.g., leaves, twigs, $n = 22$) at the National Ocean Sciences Accelerator Mass Spectrometry Facility at the Woods Hole Oceanographic Institution. Conventional radiocarbon ages were calibrated into years before 1950 CE (yBP) using IntCal13 (Reimer et al., 2013). A downcore age model was developed for each core through a Bayesian statistical approach with the R Program Bacon v2.2 (Blaauw & Christen, 2011) (Figure S2).

2.2. Historical Analysis

There is no long-term direct rainfall record for Abaco, but analysis of regional meteorological stations indicates that Nassau (New Providence Island, 25°N) and Abaco (26°N), which are separated by less than 200 km at their most distal points, experience the same hydroclimate (Jury et al., 2007). Monthly rainfall data is available from Nassau spanning the years 1855–2017 (https://climexp.knmi.nl/start.cgi). Comprehensive analysis of these historical observations required filling gaps in the record for which no monthly values were reported ($n = 141$, or 7.2% of all months). While 68% of these gaps occurred in the 19th century, more recent observations were also missing. Intermittent gaps in the rainfall record occurring after 1901 CE were filled using local precipitation reanalysis values from the University of East Anglia's Climate Research Unit (CRU TS v. 3.22; Harris et al., 2014). Missing data pre-1901 was computed using an artificial neural network curve fitting algorithm (Beale et al., 1992), in which non-linear regressions are determined by examining patterns between related input predictor datasets. To accomplish this, monthly total precipitable water (TPW) values over Nassau were extracted from the NOAA-CIRES Twentieth Century Reanalysis (V2c; Compo et al., 2011) obtained through NOAA/OAR/ESRL Physical Science Division, Boulder, Colorado, USA (https://www.esrl.noaa.gov/psd). TPW values were positively correlated with rainfall observations in Nassau ($n = 1{,}779$, $r = 0.64$, $p < 0.001$). Direct observations from the Nassau rain gauge were used to train the network and compute the missing values using the TPW predictor variable.

NASH boundary, coverage, and position information were extracted from the NOAA-CIRES Twentieth Century Reanalysis (V2c) data set. Following W. Li et al. (2011), 850 hPa geopotential height was selected as the climatic field to characterize the NASH. The boundary of the NASH was defined by identifying the 1,560 m isoline of the 850 hPa geopotential height (W. Li et al., 2011), with NASH position meaning the location of that boundary. In this study, NASH "proximity" is the *minimal distance* between the Nassau rain gauge and the 1,560 m isoline, and NASH "coverage" is defined by the *area* contained within the 1,560 m isoline. These values were computed from monthly data and then averaged over the annual wet season (MJJASO) to derive the mean NASH characteristics for each wet season. Distance and area calculations were made in ArcGIS 10.1.

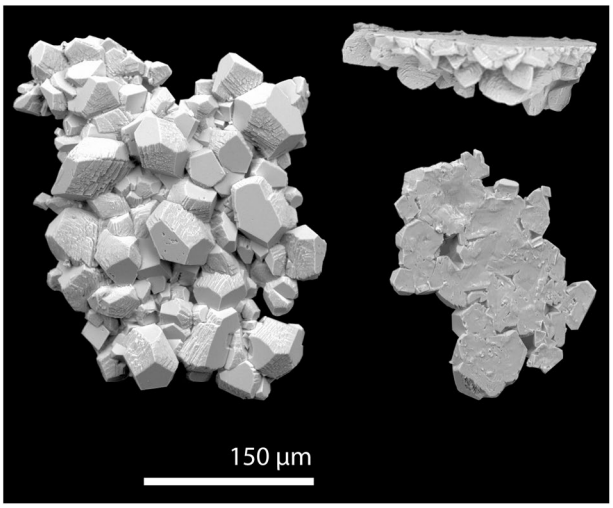

Figure 4. Scanning electron microscopic scans of calcite rafts. Top Right: Debris presented in growth position with the planar side up and dentate (subaqueous) side protruding down. Lower Right: Planar surface as viewed from above the water surface. Left: Dentate underside as viewed from below the water surface. Scans collected with a Hitachi TM3000 scanning electron microscope.

2.3. Community Earth System Model

To test the possible ocean-atmosphere dynamics that drive the hydroclimate dipole, we employed a suite of last millennium simulations from the CESM Last Millennium Ensemble (LME; Otto-Bliesner et al., 2016). Specifically, using the period 850–1849 CE for the 17 simulations that include volcanic forcing or all forcings (17,000 total years), we analyze regional climate for all 50 year periods where hydroclimate (precipitation minus evaporation, P − E) is in the top tenth percentile over the northern IAS (Abaco, 26°N) and bottom tenth percentile in the south (Grenada, 12°N), as compared to all 50 year periods where P − E is in the bottom tenth percentile in the north and top tenth percentile in the southern IAS. A suite of metrics ($n > 50$) encompassing the majority of globally and regionally important climatic features and modes of climate variability were explored for significant relationships that corresponded to these intervals. The metrics which exhibited a significant relationship were selected for discussion. It is important to note that sufficiently long forced transient simulations to analyze the timescales of interest and to cover the same time period as the reconstruction were not available for this analysis. Nevertheless, the boundary conditions are largely stable at sub-millennial scales in the middle to late Holocene, and thus multidecadal variability should be similar for the reconstructed time period and the last millennium period simulated by CESM (for further discussion, see Section S4).

3. Results

3.1. Historic Record of Regional Rainfall

Analysis of observed precipitation provides strong evidence that rainfall in the northern Bahamas is related to the geographic position of the NASH western edge. From the Nassau rain gauge (1855–2017 CE), there is a clear bimodal distribution between wet (MJJASO) and dry season (NDJFM) rainfall, and a distinct, recurrent, mid-summer drought (Figure 2e). Smoothing the Nassau record with a 10-year moving average to highlight decadal variability and minimize annual outliers from tropical cyclone events, indicates that annual precipitation totals in Nassau positively co-vary with the distance to the NASH western edge ($r = 0.46$, $p < 0.001$): mean annual rainfall over Nassau decreases (increases) the closer (further) the NASH western edge is to Nassau. The correlation is weaker over the latter half of the 20th century, perhaps owing to anthropogenically induced climate changes such as poleward shifts in the jet streams and subtropical dry zones (Fu et al., 2006), Hadley cell expansion (Seidel et al., 2008), weakening of the AMOC post-1970 (Rahmstorf et al., 2015), or warming driven variability in seasonal precipitation (Pendergrass et al., 2017; Tables S1 and S2). Indeed, modern observations show that despite a gradual local increase in annual precipitation totals in the northern Bahamas, the seasonal rainfall deficit resulting from the NASH-driven mid-summer drought has increased (Rauscher et al., 2008; Table S2). Focusing solely on the early instrumental period, before the strongest anthropogenic climate impacts (1860–1960 CE), the correlation between the distance of the NASH western edge to Nassau and Nassau rainfall increases to 0.81 ($p < 0.001$) (Figure 2f). This demonstrates that mean annual rainfall in the northern Bahamian archipelago is responsive to the proximity of the NASH western edge. Consistent with this result, rainfall over that same period exhibits a strong inverse correlation with the NASH "coverage" (i.e., spatial extent) ($r = -0.74$, $p < 0.001$). An expanded NASH enhances the local easterly trade winds, increases wind shear, and in turn lowers tropical SSTs. Lower SSTs stabilize the atmospheric boundary layer impeding convection and rainfall (L. Li et al., 2012).

3.2. Community Earth System Model Results

The CESM results (Figures 6 and S4) show that, as on shorter timescales, the hydroclimate dipole between Abaco and Grenada/Barbados on multidecadal and longer timescales is a manifestation of meridional shifts

in the location of the NASH western edge (e.g., L. Li et al., 2012). For example, when Abaco is wet and Grenada is dry, 850 hPa geopotential heights are lower over the northern Caribbean and higher over the southern Caribbean and tropical Atlantic (indicating a southern shift of the NASH western edge), and eastward trade winds in the southern Caribbean are stronger than average due to the resulting increase in the local geopotential height gradient. An analysis of regional-to-large scale modes of atmosphere and ocean variability during these periods (bottom panel of Figure 6), indicates that this regional climate pattern is closely linked to the state of the tropical and north Pacific, with a negative PDO and stronger, that is, La Ninã-like, zonal tropical Pacific temperature gradient (TPGR) correlating with the southward shift in the NASH western edge. This leads to greater moisture divergence from the region around Grenada, via the strengthened CLLJ, which when coupled with a reduced moisture supply from a contraction of the ITCZ, produces drier overall conditions in Grenada. When Abaco is dry and Grenada is wet, these modes of atmosphere and ocean variability display the opposite sign. The ITCZ expands, CLLJ relaxes, the zonal tropical Pacific temperature gradient weakens (i.e., El Ninõ-like), and the PDO enters a positive phase shifting the NASH western edge northward. While the AMO switches to a predominately positive phase during the Abaco dry/Grenada wet period (Figure S4), the average AMO state was not significantly different at the 95% level between the two periods. This indicates a weaker role for the AMO in the system.

Critically, the multidecadal and longer timescale hydroclimate dipole in the CESM is not associated with significant variations in NASH strength/intensity or shifts in the location of the NASH center (Figure S4). Nor is the dipole affected by changes in ITCZ strength or position. While there are significant differences in Hadley Cell width and the AMOC (Figure S4) during these periods, it is less clear what role these play in setting the regional climate state. While CESM struggles to reproduce aspects of the observed seasonal hydroclimatology at Abaco and Grenada, it appears to faithfully represent the observed hydroclimate dipole (Figure S5). These seasonal deviations between the model and reanalysis likely result from model bias rather than differences in the boundary conditions during the pre-industrial era. While bias issues exist in many models (Wang et al., 2014), and the results presented here are likely to be model dependent, we can have some confidence in the results provided by the CESM since the differences in Figure 6 are not expressed through changes in the seasonal cycle (Figure S6).

Finally, the modeled relationship between tropical Pacific SSTs and observed Bahamian rainfall provides additional confidence in the CESM results. As recorded by the Nassau rain gauge, mean annual rainfall totals before 1960 CE exhibit a strong inverse correlation with the Niño 3.4 index ($r = -0.72$, $n = 77$, $p < 0.05$; Table S1) when averaged on multidecadal timescales. Positive/warm phases in the Nino 3.4 region (i.e., a weaker zonal tropical Pacific temperature gradient) coinciding with reduced rainfall is consistent with the CESM and further supports the results.

3.3. Great Cistern Sedimentation

The sedimentary infill in Great Cistern primarily consists of terrestrial organic matter detritus and scattered faunal remains (including an indigenous human tibia; Sullivan et al., 2020). These organic deposits are repeatedly interrupted by pale-hued units that contain a significant increase in coarse-grained particle deposition (Figure 3). Upon microscopic inspection, these coarse-grained particles were a distinct morphology of calcite colloquially known as “calcite rafts” (Figure 4, genesis and deposition discussed further below). Found most commonly in caves, calcite rafts are sedimentary particles generated by the autochthonous $CaCO_3$ mineralization at the air-water interface of fresh to slightly oligohaline quiescent water (Fornos et al., 2009; B. Jones, 1989; Taylor & Chafetz, 2004; Taylor et al., 2004). Therefore, the downcore coarse particle variability quantifies the calcite raft deposition within Great Cistern. The Ca abundance based on XRF scanning closely follows coarse particle deposition in C2, with differences potentially related to scanning position or the 1 cm depth averaging that occurs with the lower resolution textural analysis (Figure 3). Despite the proximity of Great Cistern to the ocean, the cores contained no evidence of storm-driven overwash from the adjacent subtidal marine carbonate lagoon (e.g., relocated marine foraminifera, bivalves, or gastropods). This is likely due to the ~1.5 m elevation of the sinkhole sill coupled with its inland position on the lagoon's southern shore, where the potential impact of storm surge would be minimized.

Radiocarbon-derived age models reveal that Great Cistern preserves an oscillating record of calcite raft deposition commencing ~7,300 years ago, until calcite raft deposition ceased ~1,800 years ago. All cores display similar sedimentation rates over the last ~3 millennia (C2: 12.7 years cm^{-1}, C8: 13.0 years cm^{-1}, C7: 13.8 years cm^{-1}), however, the sedimentation rate is slower before ~3,000 years ago in C7 (25.5 years cm^{-1}). This implies that Great Cistern contains a record of sedimentation resolvable at multidecadal scales. The stratigraphic pattern is replicated, within dating uncertainties, among all three cores throughout the chronologically overlapping sediment record (3,300–1,800 yBP; Figure 2). This introduces confidence in the longer stratigraphic record of calcite raft deposition provided by C7.

Interestingly, the youngest calcite layer in all cores has a fine texture with no particles exceeding 63 μm in diameter. This layer was not identified through Sieve-first LOI analysis. However, it was evident in the XRF scanning results for C2 (Figure 3, C7: 76 cm, C2: 114 cm, C8: 135 cm core depth). From the Bayesian age modeling of the radiocarbon dates in all cores, the mean age for the cessation of this deposit is 1,590 yBP (2σ range: 1,470–1,685 yBP). This terminal horizon likely documents the final conditions favorable for calcite raft genesis but insufficient for larger particle development.

4. Great Cistern Calcite Rafts

4.1. Calcite Raft Genesis and Deposition

To interpret the calcite raft signal within Great Cistern, we must first address the separate yet related processes of calcite raft "genesis" (i.e., nucleation, development) and calcite raft "deposition" (i.e., sedimentation). Typically occurring in aqueous conditions within caves on carbonate landscapes, calcite raft genesis is largely driven by carbonate equilibrium kinetics (B. Jones, 1989; Taylor & Chafetz, 2004; Taylor et al., 2004). In general, calcite rafts form at the quiescent air-water interface of water saturated with respect to calcium carbonate, and with pCO_2 (water) greater than pCO_2 (air) (Taylor & Chafetz, 2004). As the surface water degasses, calcium carbonate saturation increases and promotes calcite raft nucleation and growth (B. Jones, 1989). For nucleation to occur the saturation index of calcite ($[\log (IAP/K_{sp})]$, expressed here as SI_C), must be greater than 0, though continued growth has been observed at slightly negative indices (Taylor & Chafetz, 2004). Buoyed by surface tension, the calcite rafts remain at the water surface where growth continues laterally and downward producing a diagnostic crystal morphology (Fornos et al., 2009; Taylor & Chafetz, 2004; van Hengstum et al., 2011) (Figure 4). Sedimentation occurs when the mass of the raft exceeds the net buoyant forces acting on it (Taylor & Chafetz, 2004), or if the surface tension is disrupted by physical action (Kovacs et al., 2017), and the raft particles sink into the benthos.

It is likely that both the onset and cessation of calcite raft genesis and deposition in Great Cistern was forced by Holocene sea-level rise. Calcite rafts most commonly occur in fresh to slightly oligohaline settings, where the ion activity and effective concentration of entrained calcium ions remain high. The reduced calcium ion activities in mesohaline to marine conditions are too low for calcite nucleation to occur ($SI_C < 0$). Inundation of the sinkhole floor by the meteoric groundwater mass would have provided the low-salinity carbonate-saturated environment necessary for calcite raft genesis (Figure 3). On porous and geologically young carbonate landscapes (e.g., eogenetic karst), the elevation of the groundwater table is closely linked to the position of local sea level (Richards et al., 1994). The elevation of the basal sediment recovered from Great Cistern was 13.5 m below modern sea level (~9 m water column, with an additional 4.5 m of sediment accumulation above the antecedent limestone). From local sea-level estimates (van Hengstum et al., 2018, 2020), and the associated effects on the vertical migration of local groundwater, the floor of Great Cistern was most likely inundated by ~7,300 yBP (Figure S3). Inundation of the shallow coastal embayment to the north of Great Cistern (Figures 2c and 2d) driven by continued Holocene sea-level rise would have caused a lateral, inland, migration of low-salinity groundwater in the subsurface (e.g., see Gulley et al., 2016). Backstepping of the meteoric lens through the antecedent carbonate, in conjunction with shoreline encroachment and eventual salinization of Great Cistern, likely prohibited larger calcite raft growth after ~1,800 yBP (Sullivan et al., 2020), with nucleation terminating entirely by ~1,600 yBP. Similar relationships between calcite raft development and meteoric groundwater rise have been previously demonstrated at Hoyo Negro cave on Mexico's Yucatan Peninsula (Collins et al., 2015) and in Green Bay Cave in Bermuda (van Hengstum et al., 2011). In both examples, flooding by rising meteoric groundwater from Holocene sea-level rise was required for calcite raft formation within the passages.

Once formation has occurred, calcite raft deposition in sinkholes may be affected by direct disturbance of the surface waters via rainfall (Kovacs et al., 2018). However, little work has been done to fully understand the relationship between calcite raft genesis, deposition, and regional hydroclimate within open-air coastal sinkholes. The most relevant work comes from Monkey Dust cave located on the Yucatan Peninsula (Kovacs et al., 2018). Despite being part of a large cave complex rather than a small coastal sinkhole, Monkey Dust is a sinkhole (i.e., cenote) that receives direct inputs of rainfall and where calcite raft deposition is influenced by seasonal rainfall variability. During a 2-year monitoring study, Kovacs et al. (2018) noted that increased rainfall led to increased rates of calcite raft sedimentation. While they did observe that increased rainfall diluted the meteoric lens within Monkey Dust (thus temporarily slowing raft genesis at the surface), the physical disturbance by the rainfall accelerated calcite raft transport into the benthos. Conversely, calcite raft deposition decreased during the dry season due to infrequent rainfall disturbances at the surface. It was also noted that evaporation during the dry season had no discernable effect on the rate of raft genesis. While one may expect that solar-induced evaporation during arid periods would encourage calcite raft formation by accelerating the rate of CO_2 degassing and increasing the $CaCO_3$ saturation (Taylor & Chafetz, 2004; Taylor et al., 2004), it is likely that this process was impeded by the continuously high relative humidity (>90%) within the cenote. These observations indicate that it cannot be assumed that rainfall suppresses calcite raft deposition, or that raft genesis is exclusively driven by solar forced evaporation in humid sinkhole environments.

Within Great Cistern, it is probable that during lower-middle and late Holocene sea-levels evaporative forcing was not the primary driver of raft genesis. Raft deposition, however, was likely driven by direct physical disturbance of the sinkhole, occurring preferentially during periods of increased rainfall. Therefore, given the temporal resolution of the record, variability in raft deposition reflects multidecadal rainfall variability over Abaco.

4.2. Calibrating Calcite Rafts to Regional Hydroclimate

To assess the fidelity of the calcite raft record as representative of regional rainfall variability, we must calibrate the Great Cistern sedimentary record to historical rainfall observations or other regionally appropriate paleo-proxy reconstructions. The broad millennial-scale decrease in the magnitude of calcite raft deposition from ~6500 to ~1,800 yBP is generally consistent with the well documented coeval reductions in summer insolation at 65°N and Caribbean rainfall during the middle to late Holocene (Fensterer et al., 2013; Haug et al., 2001; Hodell et al., 1991). Given that ~75% of the mean annual rainfall in The Bahamas occurs during the summer wet season, calcite raft deposition in Great Cistern likely reflects changes in boreal summer rainfall. Though, the 1 cm sampling interval and sedimentation rate within Great Cistern (averaged on multidecadal timescales) preclude precise disentanglement of seasonal effects on calcite raft deposition and obscure variability at finer than multidecadal resolutions. Additionally, raft deposition during the earliest portions of the record may have a different level of environmental sensitivity while the sinkhole aquatic environment was first becoming flooded by Holocene sea-level rise. However, the most significant limitation of the Great Cistern record is the lack of calcite raft debris over the last ~1,800 years, which prevents calibrating raft deposition to modern rainfall observations. Despite this limitation, we can have confidence for interpreting the long-term increases (decreases) in calcite raft deposition in Great Cistern as evidence for increased (decreased) regional rainfall through comparisons with other paleoclimate evidence from Abaco.

All cores from Great Cistern document decreased calcite raft deposition from ~3,200 to 2,500 years ago. This coincides with evidence for increasing aridity on Abaco Island, which includes expanding grasses in the understory (Slayton, 2010), abrupt stratification and salinization of a lake (van Hengstum et al., 2018) located less than 20 km from Great Cistern, and elevated δD values from native plant waxes (Tamalavage et al., 2020). Further from Abaco, Gregory et al. (2015) found increased gypsum precipitation in shallow coastal lagoons in Northern Cuba from ~3,500 to 2,500 years ago, which can also be caused by increased evaporation, decreased precipitation, and upward displacement of local saline groundwater. A long-lived Cuban speleothem at Dos Anos cave experienced a notable growth hiatus during this period (Fensterer et al., 2013), though such growth hiatuses could result from either a reduction in moisture availability or from site-specific stochastic processes. Grand-Case pond on the island of Saint-Martin (18°N) experienced prolonged lowstands between ~3,700 and 2,500 yBP as indicated by an increase in gypsum

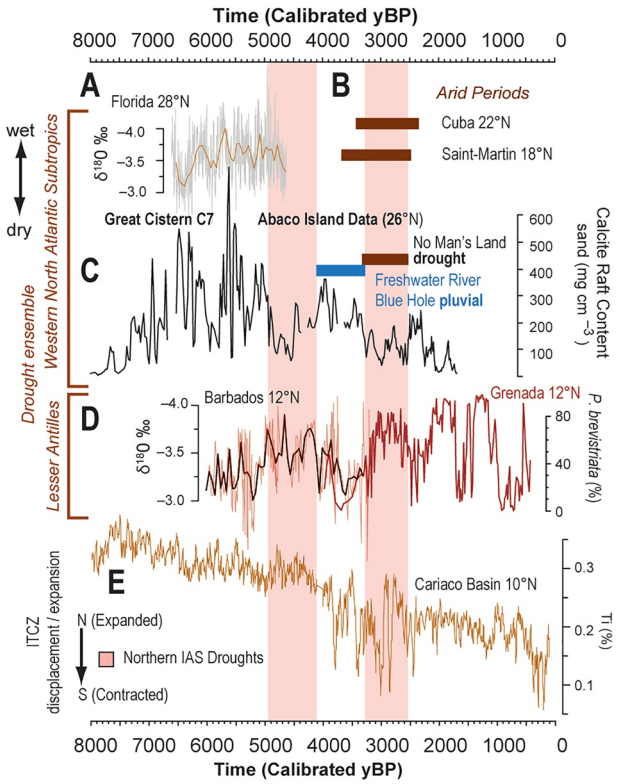

Figure 5. Hydroclimate variability in the tropical and subtropical North Atlantic Ocean. (a) Speleothem oxygen isotopic ratios from Brown's Cave (Pollock et al., 2017), (b) regional Lower-resolution record of aridity from Andros (Kjellmark, 1996), Cuba (Fensterer et al., 2013; Gregory et al., 2015), and Saint-Martin (Malaizé et al., 2011); (c) evidence for rainfall variability on Abaco Island from this study and others (van Hengstum et al., 2018, 2020), (d) Changing rainfall in the Lesser Antilles based on oxygen isotopic ratios in Harrison Cave, 50-year running mean in bold (Mangini et al., 2007) and diatoms (Fritz et al., 2011); (e) terrigenous runoff into the Cariaco Basin (Haug et al., 2001). 0 on the timeline represents 1950 CE.

and brushite evaporites in addition to floral and faunal evidence for well-oxygenated shallow waters (Malaizé et al., 2011). Contemporaneously, in the northern Gulf of Mexico, there is a sudden increase in the abundance of *Globorotalia crassaformis*, which has been interpreted as evidence of a regional-scale environmental change (Poore et al., 2003). This planktonic foraminifer is tolerant to warm/temperate and low oxygenated waters (J. I. Jones, 1966), and commonly found in upwelling regions (Lessa et al., 2020). While the environmental conditions driving the increase in *G. crassaformis* from ~3,200 to ~2,500 years ago remain uncertain, upwelling within the western Gulf is predominately wind-driven (Cochrane & Kelly, 1986; Zavala-Hidalgo et al., 2003), and the abundance of *G. crassaformis* may signify regional ocean-atmospheric adjustment related to NASH variability. In Florida, where modern rainfall is also linked to the NASH, Glaser et al. (2012) documented a marked shift to drier conditions in the Everglades after ~2,800 yBP. Slightly further inland in west-central Florida, oxygen isotopic ratios in a speleothem also suggest increased aridity between 6,000–5,800 and 5,000–4,500 years ago (Pollock et al., 2017), during which calcite raft deposition in Great Cistern decreased (Figure 5). In contrast, increased calcite raft deposition in Great Cistern from ~4,100 to 3,300 years ago corresponds with evidence for persistently wetter conditions observed elsewhere in Abaco Island. In Freshwater River Blue Hole, a stratified ~5–6 m water column shifted abruptly to well-oxygenated lacustrine conditions based on long-term stratigraphic and microfossils changes (van Hengstum et al., 2020). Wetter conditions to the south on Hispaniola have also been identified during this 800-year window, based on a shift to more depleted stable oxygen isotopic ratios preserved in lacustrine ostracodes in Lake Miragoane (Hodell et al., 1991). Earlier in the Cistern record, wetter conditions marked by a general increase in calcite raft deposition from ~7,300 to 6,500 yBP coincide with depleted stable oxygen isotopic ratios from the Dos Anos Cave speleothem in Cuba (Fensterer et al., 2013). Importantly, intervals of increased calcite raft deposition are not synchronous with periods of intense tropical cyclone activity on the western North Atlantic margin (Donnelly & Woodruff, 2007; van Hengstum et al., 2016). This means that increased calcite raft deposition is not exclusively related to increasing regional rainfall from intense tropical cyclone activity. While no metric exists to quantitatively translate calcite abundance into rainfall totals, these comparisons suggest that calcite raft deposition qualitatively reflects a positive association with rainfall amounts on multidecadal to centennial timescales.

5. Discussion

The most striking observation from our Great Cistern record is a dipole relationship between hydroclimate variability in the IAS region on centennial timescales (Figure 5). The calcite raft deposition in Great Cistern exhibits broad oscillations between periods of increased or reduced rainfall. Two such oscillations are the dry (wet) periods from 4,900 to 4,100 (4,100–3,300) and from 3,200 to 2,500 (2,500–2,300) years ago. The dipole is apparent in the contemporaneous higher/wetter (lower/drier) lake levels observed to the south in Lake Antoine, Grenada (Fritz et al., 2011) and Lake Harrison, Barbados (Mangini et al., 2007) (Figures 1b and 5). The observation of a hydroclimate dipole between the northern and southern Caribbean has been previously documented on both paleo (e.g., Fritz et al., 2011; Mangini et al., 2007) and modern (Herrera & Ault, 2017; McLean et al., 2015) timescales. This dipole is also consistent with future precipitation projections for the region (McLean et al., 2015). Annual rainfall totals are predicted to decrease in the southern Caribbean and increase in the north despite an overall decrease in summertime precipitation

(Campbell et al., 2011). The most recent illustrative example of dipole-like behavior was observed during the "Dust-Bowl" drought between 1932 and 1939 CE. This event, likely exacerbated within the United States by anthropogenic landscape modification, was primarily forced by a combination of SST anomalies within the North Atlantic and tropical Pacific (Cook et al., 2009, 2011; Cowan et al., 2020). During this period, persistent drying was spread throughout the Bahamas and southeast/central United States while increased rainfall was observed to the south in Barbados (Figure S7).

Given the disparate factors that influence Caribbean rainfall, it is unlikely that the dipole can be explained by a single climatic mechanism. The CESM results suggest that on centennial timescales, the hydroclimate dipole is driven by a combination of the position of the NASH western edge, the width of the ITCZ, and the strength of the CLLJ, which are all influenced by the state of the tropical and North Pacific. Examining the Caribbean hydroclimate reconstructions collectively, it is perhaps unsurprising that a simple comparison of the Great Cistern record to proxy records of ITCZ meridional displacement does not indicate a strong first-order qualitative correlation. More broadly, the mean latitudinal position of the Atlantic ITCZ is not a meaningful predictor of rainfall in the northern Caribbean region (Figure S4). ITCZ displacements impact moisture delivery into the southern Caribbean basin, however, the magnitude of these displacements is limited: ~±2° latitude during the historical period and ≤7° latitude in the early Holocene (Arbuszewski et al., 2013). The variability in calcite raft deposition in Great Cistern does not display any consistent correlation with middle to late Holocene meridional ITCZ displacements (Figure 5) as recorded by Ti deposition in Venezuela's Cariaco Basin (Haug et al., 2001). Increased (decreased) Ti deposition in the Cariaco Basin catchment is thought to represent increased (decreased) rainfall associated with a proximal (distal) position of the ITCZ relative to the Venezuelan coast (Figure 2b). However, highly variable Ti depositions between 3,300 to 2,500 years ago suggest frequent ITCZ repositioning during a period of more persistent arid conditions over the Little Bahama Bank (Figure 5). These comparisons suggest that ITCZ position alone does not regulate rainfall in the northern IAS.

While the ITCZ is frequently characterized by its mean meridional position, more recent work has identified its width as a salient metric. For instance, Byrne and Schneider (2016) have shown that the ITCZ narrows as the climate warms. On paleo-timelines, the distinction between Atlantic ITCZ width and ITCZ position remains to be disentangled (Arbuszewski et al., 2013; Utida et al., 2019), but ITCZ expansion/contraction does appear to be relevant to the hydroclimate dipole (Figure 6).

The multi-centennial arid intervals recorded in Great Cistern between 4,900–4,100 and 3,200–2,500 exist in stark contrast to the more frequent and more transient drier intervals prior to 5,000 yBP. The oscillations between arid and pluvial events were more frequent during the mid-Holocene. Between 6,500 and 5,000 yBP, Great Cistern indicates wetter overall conditions with intermittent centennial to multi-centennial oscillations in rainfall that exceed the magnitude of the long-term drying signal apparent over the majority of the record (~7,000–~1,800 yBP).

The transition from shorter/frequent arid events before 5000 yBP to longer/infrequent arid events afterward may reflect changes in the mean state of tropical Pacific at that time (Koutavas et al., 2006). Though the mechanisms remain unclear, an enhanced tropical Pacific zonal temperature gradient during the mid-Holocene (Barron & Anderson, 2011) correlates with increased rainfall in Abaco (as supported by the CESM). A weaker temperature gradient initiating after 5,000 yBP (Barron & Anderson, 2011; Koutavas et al., 2006) would promote aridity over the northern Bahamas while encouraging precipitation in the southern Caribbean. Decreased calcite raft deposition at Great Cistern from 4,900 to 4,100 and 3,200 to 2,500 yBP indicates a northerly shifted NASH potentially responding to changes in the state of the Pacific Ocean.

6. Conclusion

Rainfall in the IAS is modulated by meridional shifts in the position of the NASH western edge, which manifest as a hydroclimate dipole along the western margin of the tropical North Atlantic. A new middle to late Holocene precipitation record from the northern Bahamas shows multiple multi-centennial intervals of increased aridity that have impacted the northern IAS. These arid intervals are most likely produced by a northward displacement of the NASH western edge during periods of a weakened zonal tropical Pacific gradient and positive PDO-like conditions. This aridity does not appear to be influenced by the strength and/or

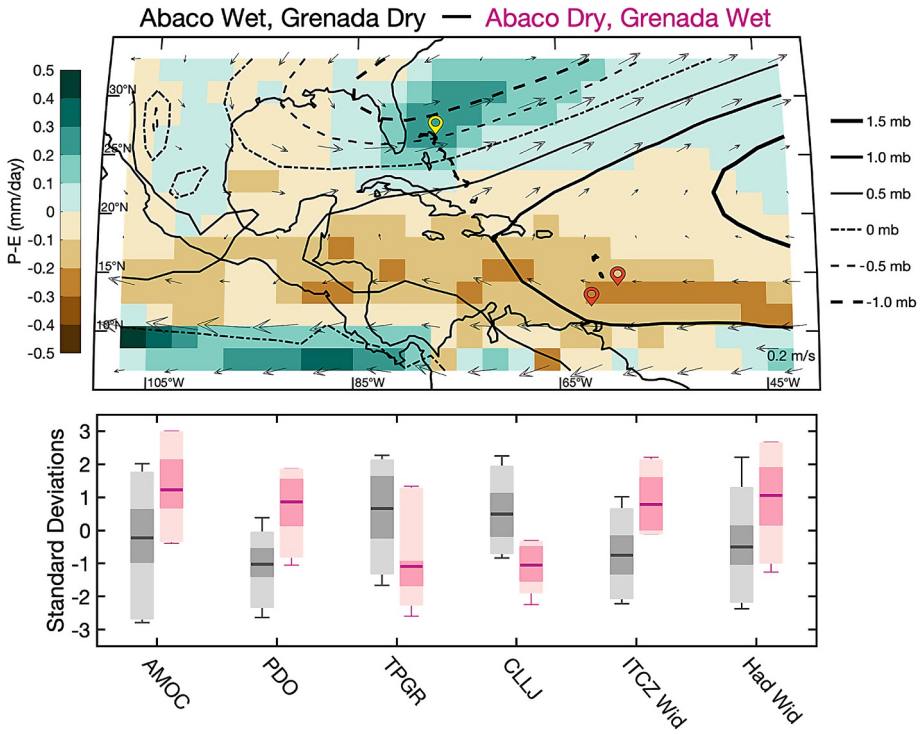

Figure 6. (Top panel) Difference in the composite 850 hPa geopotential height, 850 hPa winds, and precipitation minus evaporation (P − E) for all 50 year periods where P − E is in the top 10th percentile at Abaco, in yellow, and bottom tenth percentile at Grenada, in red (Abaco Wet, Grenada Dry—composite shown in Figure S7), and all 50-year periods where P − E is in the bottom 10th percentile at Abaco and top 10th percentile at Grenada (Abaco Dry, Grenada Wet—composite shown in Figure S5). The period 850–1849 CE for the 17 simulations that include volcanic forcing or all forcings from the Community Earth System Model (CESM) Last Millennium Ensemble (LME) were included in the analysis (17,000 total years), producing 166 Abaco Wet, Grenada Dry periods (20 fully independent) and 66 Grenada Wet, Abaco Dry periods (7 fully independent). (bottom panel) The range in the state of Atlantic Meridional Overturning Circulation (AMOC), Pacific Decadal Oscillation (PDO), Zonal Tropical Pacific Gradient (TPGR), Caribbean Low-Level Jet (CLLJ), Intertropical Convergence Zone Width (ITCZ Wid), and Hadley Cell Width (Had Wid) for Abaco Wet, Grenada Dry periods (gray) and Abaco Dry, Grenada Wet periods (magenta). Each of these has average states (thick line) for the associated 50-year periods that are significantly different at the 95% level. For the definition of these metrics, see Figure S7. The dark shaded regions represent the 25th–75th percentiles, light shaded regions the 5th–95th percentiles, and the whiskers the full range. A more comprehensive set of indices of regional-to-large scale atmosphere-ocean dynamics is shown in Figure S7, but these additional indices do not satisfy the significance criteria.

meridional position of the ITCZ. Continued anthropogenically driven changes to the NASH, the mean state and variability of the tropical Pacific, and warming North Atlantic SSTs could bring a return to these persistent arid intervals. Given the significance of Pacific forcings on NASH displacements, it becomes critically important to better assess how projected warming will influence these factors. A weaker zonal tropical Pacific temperature gradient and positive PDO-like SSTs could initiate northern dipole migration, while a stronger gradient could encourage southern dipole displacement, or minimize the impacts entirely. Therefore, a more confident assessment of the future state of the Pacific Ocean is integral for improved Caribbean hydroclimate predictions for the 21st century.

Data Availability Statement

Data sets generated during this research (grain size, chronology, and XRF) are available from the National Oceanic and Atmospheric Administration's National Centers for Environmental Information (NCEI) paleoclimatology repository (https://www.ncdc.noaa.gov/paleo/study/33492).

Acknowledgments
Laboratory and analytical assistance were provided by S. Madsen, C. Wiman, K. Kelly, V. Keeton, and S. Little. Field work was conducted with the assistance in Abaco from Friends of the Environment, D. Chamberlain, and K. Castagano. Sediment collection and export was supported by The Bahamas Environment, Science, and Technology Commission through scientific permits issued to P. J. van Hengstum and J. P. Donnelly in 2014 and 2016. This research was supported by the Texas A&M University CTE Montague Scholar Fund, the Geological Society of America Graduate Student Research Grant Program (EAR-1712071), and grants to Peter J. van Hengstum (OCE-1356509, EAR-1833117, EAR-1703087) and Jeffrey P. Donnelly (EAR-1702946) from the National Science Foundation.

References

Arbuszewski, J. A., Demenocal, P. B., Cléroux, C., Bradtmiller, L., & Mix, A. (2013). Meridional shifts of the Atlantic intertropical convergence zone since the Last Glacial Maximum. *Nature Geoscience*, *6*(11), 959–962. https://doi.org/10.1038/ngeo1961

Arienzo, M. M., Swart, P. K., Pourmand, A., Broad, K., Clement, A. C., Murphy, L. N., et al. (2015). Bahamian speleothem reveals temperature decrease associated with Heinrich stadials. *Earth and Planetary Science Letters*, *430*, 377–386. https://doi.org/10.1016/j.epsl.2015.08.035

Ashfaq, M., Rastogi, D., Mei, R., Kao, S. C., Gangrade, S., Naz, B. S., & Touma, D. (2016). High-resolution ensemble projections of near-term regional climate over the continental United States. *Journal of Geophysical Research: Atmospheres*, *121*(17), 9943–9963. https://doi.org/10.1002/2016jd025285

Barron, J. A., & Anderson, L. (2011). Enhanced late Holocene ENSO/PDO expression along the margins of the eastern North Pacific. *Quaternary International*, *235*(1–2), 3–12. https://doi.org/10.1016/j.quaint.2010.02.026

Bartlein, P. J., Anderson, K. H., Anderson, P., Edwards, M., Mock, C., Thompson, R. S., et al. (1998). Paleoclimate simulations for North America over the past 21,000 years: Features of the simulated climate and comparisons with paleoenvironmental data. *Quaternary Science Reviews*, *17*(6–7), 549–585. https://doi.org/10.1016/s0277-3791(98)00012-2

Beale, M. H., Hagan, M. T., & Demuth, H. B. (1992). *Neural network toolbox user's guide* (p. 103). The MathWorks Inc.

Blaauw, M., & Christen, J. A. (2011). Flexible paleoclimate age-depth models using an autoregressive gamma process. *Bayesian Analysis*, *6*(3), 457–474. https://doi.org/10.1214/ba/1339616472

Byrne, M. P., & Schneider, T. (2016). Narrowing of the ITCZ in a warming climate: Physical mechanisms. *Geophysical Research Letters*, *43*(21), 11–350. https://doi.org/10.1002/2016gl070396

Campbell, J. D., Taylor, M. A., Stephenson, T. S., Watson, R. A., & Whyte, F. S. (2011). Future climate of the Caribbean from a regional climate model. *International Journal of Climatology*, *31*(12), 1866–1878. https://doi.org/10.1002/joc.2200

Cochrane, J. D., & Kelly, F. J. (1986). Low-frequency circulation on the Texas-Louisiana continental shelf. *Journal of Geophysical Research: Oceans*, *91*(C9), 10645–10659. https://doi.org/10.1029/jc091ic09p10645

Collins, S. V., Reinhardt, E. G., Rissolo, D., Chatters, J. C., Blank, A. N., & Erreguerena, P. L. (2015). Reconstructing water level in Hoyo Negro, Quintana Roo, Mexico, implications for early Paleoamerican and faunal access. *Quaternary Science Reviews*, *124*, 68–83. https://doi.org/10.1016/j.quascirev.2015.06.024

Compo, G. P., Whitaker, J. S., Sardeshmukh, P. D., Matsui, N., Allan, R. J., Yin, X., et al. (2011). The twentieth century reanalysis project. *Quarterly Journal of the Royal Meteorological Society*, *137*, 1–28. https://doi.org/10.1002/qj.776

Cook, B. I., Miller, R. L., & Seager, R. (2009). Amplification of the North American "Dust Bowl" drought through human-induced land degradation. *Proceedings of the National Academy of Sciences of the United States of America*, *106*(13), 4997–5001. https://doi.org/10.1073/pnas.0810200106

Cook, B. I., Seager, R., & Miller, R. L. (2011). Atmospheric circulation anomalies during two persistent North American droughts: 1932–1939 and 1948–1957. *Climate Dynamics*, *36*(11–12), 2339–2355. https://doi.org/10.1007/s00382-010-0807-1

Cook, K. H., & Vizy, E. K. (2010). Hydrodynamics of the Caribbean low-level jet and its relationship to precipitation. *Journal of Climate*, *23*(6), 1477–1494. https://doi.org/10.1175/2009jcli3210.1

Cowan, T., Hegerl, G. C., Schurer, A., Tett, S. F., Vautard, R., Yiou, P., et al. (2020). Ocean and land forcing of the record-breaking Dust Bowl heatwaves across central United States. *Nature Communications*, *11*(1), 1–9. https://doi.org/10.1038/s41467-020-16676-w

Donnelly, J. P., & Woodruff, J. D. (2007). Intense hurricane activity over the past 5,000 years controlled by El Niño and the West African monsoon. *Nature*, *447*(7143), 465–468. https://doi.org/10.1038/nature05834

Easterling, D. R., Kunkel, K., Arnold, J., Knutson, T., LeGrande, A., Leung, L. R., et al. (2017). *Precipitation change in the United States*. United States Department of Commerce.

Fall, P. L., van Hengstum, P. J., Lavold-Foote, L., Donnelly, J. P., Albury, N. A., & Tamalavage, A. E. (2021). Human arrival and landscape dynamics in the northern Bahamas. *Proceedings of the National Academy of Sciences of the United States of America*, *118*(10). https://doi.org/10.1073/pnas.2015764118

Fensterer, C., Scholz, D., Hoffmann, D. L., Spötl, C., Schröder-Ritzrau, A., Horn, C., et al. (2013). Millennial-scale climate variability during the last 12.5 ka recorded in a Caribbean speleothem. *Earth and Planetary Science Letters*, *361*, 143–151. https://doi.org/10.1016/j.epsl.2012.11.019

Fornos, J. J., Gines, J., & Gracia, F. (2009). Present-day sedimentary facies in the coastal karst caves of Mallorca island (western Mediterranean). *Journal of Cave and Karst Studies*, *71*(1), 86–99.

Fritz, S. C., Björck, S., Rigsby, C. A., Baker, P. A., Calder-Church, A., & Conley, D. J. (2011). Caribbean hydrological variability during the Holocene as reconstructed from crater lakes on the island of Grenada. *Journal of Quaternary Science*, *26*(8), 829–838. https://doi.org/10.1002/jqs.1512

Fu, Q., Johanson, C. M., Wallace, J. M., & Reichler, T. (2006). Enhanced mid-latitude tropospheric warming in satellite measurements. *Science*, *312*(5777), 1179. https://doi.org/10.1126/science.1125566

Gamble, D. W., Parnell, D. B., & Curtis, S. (2008). Spatial variability of the Caribbean mid-summer drought and relation to north Atlantic high circulation. *International Journal of Climatology: A Journal of the Royal Meteorological Society*, *28*(3), 343–350. https://doi.org/10.1002/joc.1600

Glaser, P. H., Hansen, B. C. S., Donovan, J. J., Givnish, T. J., Stricker, C. A., & Volin, J. C. (2012). Holocene dynamics of the Florida Everglades with respect to climate, dustfall, and tropical storms. *Proceedings of the National Academy of Sciences of the United States of America*, *110*(43), 17211–17216.

Gregory, B. R. B., Peros, M., Reinhardt, E. G., & Donnelly, J. P. (2015). Middle-late Holocene Caribbean aridity inferred from foraminifera and elemental data in sediment cores from two Cuban lagoons. *Paleogeography, Palaeoclimatology, Palaeoecology*, *426*, 229–241. https://doi.org/10.1016/j.palaeo.2015.02.029

Gulley, J. D., Mayer, A. S., Martin, J. B., & Bedekar, V. (2016). Sea level rise and inundation of island interiors: Assessing impacts of lake formation and evaporation on water resources in arid climates. *Geophysical Research Letters*, *43*, 9712–9719. https://doi.org/10.1002/2016gl070667

Harris, I. P. D. J., Jones, P. D., Osborn, T. J., & Lister, D. H. (2014). Updated high-resolution grids of monthly climatic observations—The CRU TS3. 10 dataset. *International Journal of Climatology*, *34*(3), 623–642. https://doi.org/10.1002/joc.3711

Hastenrath, S. (1976). Variations in low-latitude circulation and extreme climatic events in the tropical Americas. *Journal of the Atmospheric Sciences*, *33*, 202–215. https://doi.org/10.1175/1520-0469(1976)033<0202:villca>2.0.co;2

Hastenrath, S. (1984). Interannual variability and annual cycle: Mechanisms of circulation and climate in the tropical Atlantic Sector. *Monthly Weather Review*, *112*, 1097–1107. https://doi.org/10.1175/1520-0493(1984)112<1097:ivaacm>2.0.co;2
Haug, G. H., Hughen, K. A., Sigman, D. M., Peterson, L. C., & Röhl, U. (2001). Southward migration of the intertropical convergence zone through the Holocene. *Science*, *293*(5533), 1304–1308. https://doi.org/10.1126/science.1059725
Hay, J. E., Forbes, D. L., & Mimura, N. (2013). Understanding and managing global change in small islands. *Sustainability Science*, *8*(3), 303–308. https://doi.org/10.1007/s11625-013-0220-x
Herrera, D., & Ault, T. (2017). Insights from a new high-resolution drought atlas for the Caribbean spanning 1950–2016. *Journal of Climate*, *30*(19), 7801–7825. https://doi.org/10.1175/jcli-d-16-0838.1
Hodell, D. A., Curtis, J. H., Jones, G. A., Higuera-Gundy, A., Brenner, M., Binford, M. W., & Dorsey, K. T. (1991). Reconstruction of Caribbean climate change over the past 10,000 years. *Nature*, *352*, 790–793. https://doi.org/10.1038/352790a0
Hu, Q., Feng, S., & Oglesby, R. J. (2011). Variations in North American summer precipitation driven by the Atlantic multidecadal oscillation. *Journal of Climate*, *24*(21), 5555–5570. https://doi.org/10.1175/2011jcli4060.1
Jones, B. (1989). Calcite rafts, peloids, and micrite in cave deposits from Cayman Brae, British West Indies. *Canadian Journal of Earth Sciences*, *26*(4), 654–664. https://doi.org/10.1139/e89-056
Jones, J. I. (1966). Significance of distribution of planktonic foraminifera in equatorial Atlantic undercurrent. *AAPG Bulletin*, *50*(3), 619. https://doi.org/10.1306/5d25b51b-16c1-11d7-8645000102c1865d
Jury, M., Malmgren, B. A., & Winter, A. (2007). Subregional precipitation climate of the Caribbean and relationships with ENSO and NAO. *Journal of Geophysical Research*, *112*(D16). https://doi.org/10.1029/2006jd007541
Karnauskas, K. B., Donnelly, J. P., & Anchukaitis, K. J. (2016). Future freshwater stress for island populations. *Nature Climate Change*, *6*(7), 720–725. https://doi.org/10.1038/nclimate2987
Kelly, P., Kravitz, B., Lu, J., & Leung, L. R. (2018). Remote drying in the North Atlantic as a common response to precessional changes and CO_2 increase over land. *Geophysical Research Letters*, *45*(8), 3615–3624. https://doi.org/10.1002/2017gl076669
Kelman, I., & West, J. J. (2009). Climate change and small island developing states: A critical review. *Ecological and Environmental Anthropology*, *5*(1), 1–16.
Kjellmark, E. (1996). Late Holocene climate change and human disturbance on Andros Island, Bahamas. *Journal of Paleolimnology*, *15*(2), 133–145. https://doi.org/10.1007/bf00196777
Koutavas, A., Demenocal, P. B., Olive, G. C., & Lynch-Stieglitz, J. (2006). Mid-Holocene El Niño-Southern Oscillation (ENSO) attenuation revealed by individual foraminifera in eastern tropical Pacific sediments. *Geology*, *34*(12), 993–996. https://doi.org/10.1130/g22810a.1
Kovacs, S. E., Reinhardt, E. G., Chatters, J. C., Rissolo, D., Schwarcz, H. P., Collins, S. V., et al. (2017). Calcite raft geochemistry as a hydrological proxy for Holocene aquifer conditions in Hoyo Negro and Ich Balam (Sac Actun Cave System), Quintana Roo, Mexico. *Quaternary Science Reviews*, *175*, 97–111. https://doi.org/10.1016/j.quascirev.2017.09.006
Kovacs, S. E., Reinhardt, E. G., Werner, C., Kim, S. T., Devos, F., & Le Maillot, C. (2018). Seasonal trends in calcite-raft precipitation from cenotes Rainbow, Feno and Monkey Dust, Quintana Roo, Mexico: Implications for paleoenvironmental studies. *Palaeogeography, Palaeoclimatology, Palaeoecology*, *497*, 157–167. https://doi.org/10.1016/j.palaeo.2018.02.014
Lessa, D., Morard, R., Jonkers, L., Venancio, I. M., Reuter, R., Baumeister, A., et al. (2020). Distribution of planktonic foraminifera in the subtropical South Atlantic: Depth hierarchy of controlling factors. *Biogeosciences*, *17*(16), 4313–4342. https://doi.org/10.5194/bg-17-4313-2020
Li, L., Li, W., & Kushnir, Y. (2012). Variation of the North Atlantic subtropical high western ridge and its implication to southeastern US summer precipitation. *Climate Dynamics*, *39*, 1401–1412. https://doi.org/10.1007/s00382-011-1214-y
Li, W., Li, L., Fu, R., Deng, Y., & Wang, H. (2011). Changes to the North Atlantic subtropical high and its role in the intensification of summer rainfall variability in the southeastern United States. *Journal of Climate*, *24*(5), 1499–1506. https://doi.org/10.1175/2010jcli3829.1
Li, W., Li, L., Ting, M., & Liu, Y. (2012). Intensification of Northern Hemisphere subtropical highs in a warming climate. *Nature Geoscience*, *5*, 830–834. https://doi.org/10.1038/ngeo1590
Lu, J., Vecchi, G. A., & Reichler, T. (2007). Expansion of the Hadley cell under global warming. *Geophysical Research Letters*, *34*(6). https://doi.org/10.1029/2007gl030931
Malaizé, B., Bertran, P., Carbonel, P., Bonnissent, D., Charlier, K., Galop, D., et al. (2011). Hurricanes and climate in the Caribbean during the past 3700 years BP. *The Holocene*, *21*(6), 911–924. https://doi.org/10.1177/0959683611400198
Mangini, A., Blumbach, P., Verdes, P., Spötl, C., Scholz, D., Machel, H., & Mahon, S. (2007). Combined records from a stalagmite from Barbados and from lake sediments in Haiti reveal variable seasonality in the Caribbean between 6.7 and 3 ka BP. *Quaternary Science Reviews*, *26*(9–10), 1332–1343. https://doi.org/10.1016/j.quascirev.2007.01.011
Martin, E. R., & Schumacher, C. (2011). The Caribbean low-level jet and its relationship with precipitation in IPCC AR4 models. *Journal of Climate*, *24*(22), 5935–5950. https://doi.org/10.1175/jcli-d-11-00134.1
Martinez, C., Goddard, L., Kushnir, Y., & Ting, M. (2019). Seasonal climatology and dynamical mechanisms of rainfall in the Caribbean. *Climate Dynamics*, *53*(1), 825–846.
Mayewski, P. A., Rohling, E. E., Stager, J. C., Karlén, W., Maasch, K. A., Meeker, L. D., et al. (2004). Holocene climate variability. *Quaternary Research*, *62*(3), 243–255. https://doi.org/10.1016/j.yqres.2004.07.001
McLean, N. M., Stephenson, T. S., Taylor, M. A., & Campbell, J. D. (2015). Characterization of future Caribbean rainfall and temperature extremes across rainfall zones. *Advances in Meteorology*. 425987. https://doi.org/10.1155/2015/425987
Moreno-Chamarro, E., Marshall, J., & Delworth, T. L. (2020). Linking ITCZ migrations to the AMOC and North Atlantic/Pacific SST decadal variability. *Journal of Climate*, *33*(3), 893–905. https://doi.org/10.1175/jcli-d-19-0258.1
Naumann, G., Alfieri, L., Wyser, K., Mentaschi, L., Betts, R. A., Carrao, H., et al. (2018). Global changes in drought conditions under different levels of warming. *Geophysical Research Letters*, *45*(7), 3285–3296. https://doi.org/10.1002/2017gl076521
Otto-Bliesner, B. L., Brady, E. C., Fasullo, J., Jahn, A., Landrum, L., Stevenson, S., et al. (2016). Climate variability and change since 850 CE: An ensemble approach with the Community Earth System Model. *Bulletin of the American Meteorological Society*, *97*(5), 735–754. https://doi.org/10.1175/bams-d-14-00233.1
Pelling, M., & Uitto, J. I. (2001). Small island developing states: Natural disaster vulnerability and global change. *Environmental Hazards*, *3*, 49–62. https://doi.org/10.1016/s1464-2867(01)00018-3
Pendergrass, A. G., Knutti, R., Lehner, F., Deser, C., & Sanderson, B. M. (2017). Precipitation variability increases in a warmer climate. *Scientific Reports*, *7*(1), 17966. https://doi.org/10.1038/s41598-017-17966-y
Pollock, A. L., van Beynen, P. E., DeLong, K. L., Polyak, V., & Asmerom, Y. (2017). A speleothem-based mid-Holocene precipitation reconstruction for West-Central Florida. *The Holocene*, *27*(7), 987–996. https://doi.org/10.1177/0959683616678463

Poore, R. Z., Dowsett, H. J., Verardo, S., & Quinn, T. M. (2003). Millennial-to century-scale variability in Gulf of Mexico Holocene climate records. *Paleoceanography*, *18*(2). https://doi.org/10.1029/2002pa000868

Prudhomme, C., Giuntoli, I., Robinson, E. L., Clark, D. B., Arnell, N. W., Dankers, R., et al. (2014). Hydrological droughts in the 21st century, hotspots and uncertainties from a global multimodel ensemble experiment. *Proceedings of the National Academy of Sciences of the United States of America*, *111*(9), 3262–3267. https://doi.org/10.1073/pnas.1222473110

Rahmstorf, S., Box, J. E., Feulner, G., Mann, M. E., Robinson, A., Rutherford, S., & Schaffernicht, E. J. (2015). Exceptional twentieth-century slowdown in Atlantic Ocean overturning circulation. *Nature Climate Change*, *5*(5), 475–480. https://doi.org/10.1038/nclimate2554

Rauscher, S. A., Giorgi, F., Diffenbaugh, N. S., & Seth, A. (2008). Extension and intensification of the Meso-American mid-summer drought in the twenty-first century. *Climate Dynamics*, *31*(5), 551–571. https://doi.org/10.1007/s00382-007-0359-1

Reimer, P. J., Bard, E., Bayliss, A., Beck, J. W., Blackwell, P. G., Ramsey, C. B., et al. (2013). IntCal13 and Marine13 radiocarbon age calibration curves 0–50,000 years cal BP. *Radiocarbon*, *55*(4), 1869–1887. https://doi.org/10.2458/azu_js_rc.55.16947

Richards, D. A., Smart, P. L., & Edwards, R. L. (1994). Maximum sea levels for the last glacial period from U-series ages of submerged speleothems. *Nature*, *367*(6461), 357–360. https://doi.org/10.1038/367357a0

Routson, C. C., McKay, N. P., Kaufman, D. S., Erb, M. P., Goosse, H., Shuman, B. N., et al. (2019). Mid-latitude net precipitation decreased with Arctic warming during the Holocene. *Nature*, *568*(7750), 83–87. https://doi.org/10.1038/s41586-019-1060-3

Scheff, J., & Frierson, D. M. (2012). Robust future precipitation declines in CMIP5 largely reflect the poleward expansion of model subtropical dry zones. *Geophysical Research Letters*, *39*(18). https://doi.org/10.1029/2012gl052910

Seidel, D. J., Fu, Q., Randel, W. J., & Reichler, T. J. (2008). Widening of the tropical belt in a changing climate. *Nature Geoscience*, *1*(1), 21–24. https://doi.org/10.1038/ngeo.2007.38

Slayton, I. A. (2010). *A vegetation history from Emerald Pond, Great Abaco Island, the Bahamas, based on pollen analysis (Master's Thesis)* (p. 85). University of Tennessee.

Sullivan, R. M., van Hengstum, P. J., Donnelly, J. P., Winkler, T. S., Mark, S. E., & Albury, N. A. (2020). Absolute and relative dating of human remains in a Bahamian sinkhole (Great Cistern, Abaco). *Journal of Archaeological Science: Reports*, *32*, 102441. https://doi.org/10.1016/j.jasrep.2020.102441

Tamalavage, A. E., van Hengstum, P. J., Louchouarn, P., Fall, P. L., Donnelly, J. P., Albury, N. A., et al. (2020). Plant wax evidence for precipitation and vegetation change from a coastal sinkhole lake in the Bahamas spanning the last 3000 years. *Organic Geochemistry*, *150*, 104120. https://doi.org/10.1016/j.orggeochem.2020.104120

Taylor, M. P., Drysdale, R. N., & Carthew, K. D. (2004). The formation and environmental significance of calcite rafts in tropical tufa-depositing rivers of northern Australia. *Sedimentology*, *51*(5), 1089–1101. https://doi.org/10.1111/j.1365-3091.2004.00661.x

Taylor, P. M., & Chafetz, H. S. (2004). Floating rafts of calcite crystals in cave pools, central Texas, USA: Crystal habit vs. saturation state. *Journal of Sedimentary Research*, *74*(3), 328–341. https://doi.org/10.1306/111603740328

Utida, G., Cruz, F. W., Etourneau, J., Bouloubassi, I., Schefuß, E., Vuille, M., et al. (2019). Tropical South Atlantic influence on northeastern Brazil precipitation and ITCZ displacement during the past 2300 years. *Scientific Reports*, *9*(1), 1–8. https://doi.org/10.1038/s41598-018-38003-6

van Hengstum, P. J., Donnelly, J. P., Fall, P. L., Toomey, M. R., Albury, N. A., & Kakuk, B. (2016). The intertropical convergence zone modulates intense hurricane strikes on the western North Atlantic margin. *Scientific Reports*, *6*, 21728. https://doi.org/10.1038/srep21728

van Hengstum, P. J., Maale, G., Donnelly, J. P., Albury, N. A., Onac, B. P., Sullivan, R. M., et al. (2018). Drought in the northern Bahamas from 3300 to 2500 years ago. *Quaternary Science Reviews*, *186*, 169–185. https://doi.org/10.1016/j.quascirev.2018.02.014

van Hengstum, P. J., Scott, D. B., Grocke, D. R., & Charette, M. A. (2011). Sea level controls sedimentation and environments in coastal caves and sinkholes. *Marine Geology*, *286*, 35–50. https://doi.org/10.1016/j.margeo.2011.05.004

van Hengstum, P. J., Winkler, T. S., Tamalavage, A. E., Sullivan, R. M., Little, S. N., MacDonald, D., et al. (2020). Holocene sedimentation in a blue hole surrounded by carbonate tidal flats in The Bahamas: Autogenic versus allogenic processes. *Marine Geology*, *419*, 106051. https://doi.org/10.1016/j.margeo.2019.106051

Wang, C., Zhang, L., Lee, S. K., Wu, L., & Mechoso, C. R. (2014). A global perspective on CMIP5 climate model biases. *Nature Climate Change*, *4*(3), 201–205. https://doi.org/10.1038/nclimate2118

Zavala-Hidalgo, J., Morey, S. L., & O'Brien, J. J. (2003). Seasonal circulation on the western shelf of the Gulf of Mexico using a high-resolution numerical model. *Journal of Geophysical Research*, *108*(C12).

References From the Supporting Information

Byrne, M. P., Pendergrass, A. G., Rapp, A. D., & Wodzicki, K. R. (2018). Response of the intertropical convergence zone to climate change: Location, width, and strength. *Current Climate Change Reports*, *4*(4), 355–370. https://doi.org/10.1007/s40641-018-0110-5

Coats, S., & Karnauskas, K. B. (2017). Are simulated and observed twentieth century tropical Pacific sea surface temperature trends significant relative to internal variability? *Geophysical Research Letters*, *44*(19), 9928–9937. https://doi.org/10.1002/2017gl074622

Dandoy, S., Pausata, F. S., Camargo, S. J., Laprise, R., Winger, K., & Emanuel, K. (2021). Atlantic hurricane response to Saharan greening and reduced dust emissions during the mid-Holocene. *Climate of the Past*, *17*(2), 675–701. https://doi.org/10.5194/cp-17-675-2021

Giannini, A., Kushnir, Y., & Cane, M. (2001). Seasonality in the impact of ENSO and the North Atlantic high on Caribbean rainfall. *Physics and Chemistry of the Earth—Part B: Hydrology, Oceans and Atmosphere*, *26*(2), 143–147. https://doi.org/10.1016/s1464-1909(00)00231-8

Harrison, S. P., Bartlein, P. J., Izumi, K., Li, G., Annan, J., Hargreaves, J., et al. (2015). Evaluation of CMIP5 palaeo-simulations to improve climate projections. *Nature Climate Change*, *5*(8), 735–743. https://doi.org/10.1038/nclimate2649

Khan, N. S., Ashe, E., Horton, B. P., Dutton, A., Kopp, R. E., Brocard, G., et al. (2017). Drivers of Holocene sea-level change in the Caribbean. *Quaternary Science Reviews*, *155*, 13–36. https://doi.org/10.1016/j.quascirev.2016.08.032

Mantsis, D. F., Clement, A. C., Kirtman, B., Broccoli, A. J., & Erb, M. P. (2013). Precessional cycles and their influence on the North Pacific and North Atlantic summer anticyclones. *Journal of Climate*, *26*(13), 4596–4611. https://doi.org/10.1175/jcli-d-12-00343.1

Mantua, N. J., Hare, S. R., Zhang, Y., Wallace, J. M., & Francis, R. C. (1997). A Pacific interdecadal climate oscillation with impacts on salmon production. *Bulletin of the American Meteorological Society*, *78*(6), 1069–1079. https://doi.org/10.1175/1520-0477(1997)078<1069:apicow>2.0.co;2

Milne, G. A., & Peros, M. (2013). Data–model comparison of Holocene sea-level change in the circum-Caribbean region. *Global and Planetary Change*, *107*, 119–131. https://doi.org/10.1016/j.gloplacha.2013.04.014

Neumann, A. C., & Land, L. S. (1975). Lime mud deposition and calcareous algae in the Bight of Abaco, Bahamas; a budget. *Journal of Sedimentary Research*, *45*(4), 763–786. https://doi.org/10.1306/212f6e3d-2b24-11d7-8648000102c1865d

Pausata, F. S., Zhang, Q., Muschitiello, F., Lu, Z., Chafik, L., Niedermeyer, E. M., et al. (2017). Greening of the Sahara suppressed ENSO activity during the mid-Holocene. *Nature Communications*, *8*(1), 1–12. https://doi.org/10.1038/ncomms16020

Rasmussen, K. A., Haddad, R. I., & Neumann, A. C. (1990). Stable-isotope record of organic carbon from an evolving carbonate banktop, Bight of Abaco, Bahamas. *Geology*, *18*(8), 790–794. https://doi.org/10.1130/0091-7613(1990)018<0790:sirooc>2.3.co;2

Rayner, N. A. A., Parker, D. E., Horton, E. B., Folland, C. K., Alexander, L. V., Rowell, D. P., et al. (2003). Global analyses of sea surface temperature, sea ice, and night marine air temperature since the late nineteenth century. *Journal of Geophysical Research*, *108*(D14). https://doi.org/10.1029/2002jd002670

Trenberth, K. E., & Shea, D. J. (2006). Atlantic hurricanes and natural variability in 2005. *Geophysical Research Letters*, *33*(12). https://doi.org/10.1029/2006gl026894

Wang, C. (2007). Variability of the Caribbean low-level jet and its relations to climate. *Climate Dynamics*, *29*(4), 411–422. https://doi.org/10.1007/s00382-007-0243-z